Loss of AKAP1 triggers Drp1 dephosphorylation-mediated mitochondrial fission and loss in retinal ganglion cells

Genea Edwards,[1*] Guy A. Perkins,[2*] Keun-Young Kim,[2*] YeEun Kong,[1] Yonghoon Lee,[1] Soo-Ho Choi,[3] Yujia Liu,[4] Dorota Skowronska-Krawczyk,[1] Robert N. Weinreb,[1] Linda Zangwill,[1] Stefan Strack[4] and Won-Kyu Ju[1]

[1]Hamilton Glaucoma Center and Viterbi Family Department of Ophthalmology, Shiley Eye Institute, University of California San Diego, La Jolla, CA, USA

[2]National Center for Microscopy and Imaging Research and Department of Neuroscience, University of California San Diego, La Jolla, CA, USA

[3]Department of Medicine, University of California San Diego, La Jolla, CA, USA

[4]Department of Pharmacology and Iowa Neuroscience Institute, University of Iowa, Iowa City, IA, USA

Running title: Loss of AKAP1 in retinal ganglion cells

*Genea Edwards, Guy A. Perkins and Keun-Young Kim contributed equally to this work.

Corresponding author: Won-Kyu Ju, Ph.D.
Hamilton Glaucoma Center
Viterbi Family Department of Ophthalmology
Shiley Eye Institute
University of California, San Diego
9415 Campus Point Drive
La Jolla, CA 92037
Email: wju@ucsd.edu

Abstract

Impairment of mitochondrial structure and function is strongly linked to glaucoma pathogenesis. Despite the widely appreciated disease relevance of mitochondrial dysfunction and loss, the molecular mechanisms underlying mitochondrial fragmentation and metabolic stress in glaucoma are poorly understood. We demonstrate here that glaucomatous retinal ganglion cells (RGCs) show loss of A-kinase anchoring protein 1 (AKAP1), activation of calcineurin (CaN) and reduction of dynamin-related protein 1 (Drp1) phosphorylation at serine 637 (Ser637). These findings suggest that AKAP1-mediated phosphorylation of Drp1 at Ser637 has a critical role in RGC survival in glaucomatous neurodegeneration. Male mice lacking AKAP1 show increases of CaN and total Drp1 level, as well as a decrease of Drp1 phosphorylation at Ser637 in the retina. Ultrastructural analysis of mitochondria shows that loss of AKAP1 triggers mitochondrial fragmentation and loss, as well as mitophagosome formation in RGCs. Loss of AKAP1 deregulates oxidative phosphorylation (OXPHOS) complexes (Cxs) by increasing CxII and decreasing CxIII-V, leading to metabolic and oxidative stress. Also, loss of AKAP1 decreases Akt phosphorylation at Serine 473 (Ser473) and threonine 308 (Thr308) and activates the Bim/Bax signaling pathway in the retina. These results suggest that loss of AKAP1 has a critical role in RGC dysfunction by decreasing Drp1 phosphorylation at Ser637, deregulating OXPHOS, decreasing Akt phosphorylation at Ser473 and Thr308, and activating the Bim/Bax pathway in glaucomatous neurodegeneration. Thus, we propose that overexpression of AKAP1 or modulation of Drp1 phosphorylation at Ser637 are potential therapeutic strategies for neuroprotective intervention in glaucoma and other mitochondria-related optic neuropathies.

63 **Introduction**

64 Primary open-angle glaucoma (POAG) is characterized by a slow and progressive degeneration
65 of retinal ganglion cells (RGCs) and their axons, leading to loss of visual function[1]. The factors
66 contributing to degeneration of the RGC and its axon degeneration in POAG are not well
67 understood. Recent studies have shown that POAG patients have mitochondrial abnormalities[2-7].
68 Evidence from our group and others indicates that compromised mitochondrial dynamics,
69 metabolic stress and mitochondrial dysfunction by glaucomatous insults such as elevated
70 intraocular pressure (IOP) and oxidative stress are critical to RGC loss in experimental
71 glaucoma[8-14]. Despite the widely appreciated disease relevance of mitochondrial dysfunction
72 and loss, the molecular mechanisms underlying the impairment of mitochondrial structure and
73 function in glaucoma are poorly understood.

74 A-kinase anchoring protein 1 (AKAP1), a scaffold protein, is part of the elaborate
75 architecture which binds to the regulatory subunit of protein kinase A (PKA) along with other
76 signaling molecules such as Src kinase, protein phosphatase 1 (PP1), Ca^{2+}-dependent
77 phosphatase calcineurin (CaN) and phosphodiesterase 4 (PDE4)[15-20]. By recruiting the PKA
78 holoenzyme to the outer mitochondrial membrane (OMM), AKAP1 is strategically positioned to
79 integrate multiple signal transduction cascades, including cyclic adenosine 3´5´-monophosphate
80 (cAMP) signaling, in the regulation of mitochondrial shape and function. AKAP1 facilitates
81 dynamin-related protein 1 (Drp1) phosphorylation and subsequent mitochondrial elongation. It
82 also increases adenosine triphosphate (ATP) generation and mitochondrial membrane
83 potential[21,22], and these collective changes are neuroprotective [23,24]. Emerging evidence
84 indicates that AKAP1 protects from cerebral ischemic stroke by maintaining respiratory chain
85 activity, inhibiting Drp1 dependent mitochondrial fission and superoxide production, and
86 delaying Ca^{2+} deregulation [24].

87 Excessive mitochondrial fission-mediated dysfunction has been implicated in various
88 neurodegenerative diseases including glaucoma[8,11,25,26]. Complexes of Drp1 assemble from the
89 cytosol onto mitochondria at focal sites of mitochondrial fission[27,28]. Recent evidence indicates
90 that post-translational modifications of Drp1 are linked to mitochondrial dysfunction-mediated
91 bioenergetic failure, synaptic injury and neuronal cell death[25,29-32]. Phosphorylation of Drp1 at
92 serine 637 (Ser637) by the cAMP-dependent PKA promotes mitochondrial fusion, whereas
93 dephosphorylation by the CaN promotes mitochondrial fission by decreasing Drp1 activity[33-35].

94 Previous studies showed that inhibition of Drp1 activity prevents mitochondrial fission and
95 protects RGCs and their axons in experimental glaucoma[11,36,37]. However, it remains unknown
96 whether AKAP1-mediated Drp1 phosphorylation at Ser637 play a critical role in glaucomatous
97 neurodegeneration. Along this line, the existence of AKAP1 in RGCs and its role in glaucoma
98 are completely unknown.
99 To address these questions, we investigated AKAP1 protein expression and Drp1
100 phosphorylation at Ser637 in retinas from glaucomatous DBA/2J mice, and also evaluated the
101 effect of AKAP1 loss in the retina using AKAP1 knockout ($AKAP1^{-/-}$) mice.
102
103
104
105
106
107
108
109
110
111
112
113
114
115
116
117
118
119
120
121
122
123
124

125 **Results**

126 **AKAP1 deficiency in glaucomatous RGCs.**

127 We examined AKAP1 protein expression in the retina of a mouse model of glaucoma DBA/2J
128 mice, which spontaneously develop elevated IOP and glaucomatous damage with age[8,11,38].
129 Control DBA/2J-*Gpnmb*$^{+}$*/SjJ* (D2-*Gpnmb*$^{+}$) was used in which the gene for Gpnmb that has
130 been altered to wild type sequence by targeted gene mutation. It is otherwise identical to the
131 DBA/2J mouse strain, but maintains normal IOP during aging and does not develop optic nerve
132 axon loss[39,40]. Our results demonstrated for the first time that elevated IOP significantly
133 decreased AKAP1 protein expression in the retinas of 10-month-old glaucomatous DBA/2J mice
134 compared with the retina of age-matched control D2-*Gpnmb*$^{+}$ mice (Fig. 1a). We observed that
135 AKAP1 immunoreactivity was highly present in the outer plexiform layer (OPL) and ganglion
136 cell layer (GCL) in D2-*Gpnmb*$^{+}$ retina (Fig. 1b). More specifically, AKAP1 immunoreactivity
137 was colocalized with neuronal class III β-tubulin (TUJ1)-positive RGCs in the GCL of D2-
138 *Gpnmb*$^{+}$ retina. Of interest, however, AKAP1 immunoreactivity was decreased in the OPL and
139 TUJ1-positive RGCs in the GCL of glaucomatous DBA/2J retina (Fig. 1b and c).

140

141 **Activation of CaN and dephosphorylation of Drp1 at Ser637 in glaucomatous retina**

142 AKAP1 binds with two Serine/Threonine phosphatases, PP1 and CaN[41,42]. Loss of AKAP1
143 causes Drp1-mediated mitochondrial fission and decreases Drp1phsophorylation at Ser637 in
144 neuronal cells of the brain[21,23,24,43,44]. More importantly, AKAP1 protects brain neuronal cells
145 against cerebral ischemic stroke by inhibiting Drp1-dependent mitochondrial fission[24]. Since
146 elevated IOP increased CaN and total Drp1 protein expression[11,45], as well as Drp1 inhibition
147 rescued RGCs and their axons by preserving mitochondrial integrity in the retina and/or glial
148 lamina of glaucomatous DBA/2J mice[11], we examined the expression levels of CaN and total
149 Drp1, as well as phosphorylation of Drp1 at Ser637 in the retina of 10-month-old glaucomatous
150 DBA/2J mice. We observed a significant increase of CaN protein expression in glaucomatous
151 DBA/2J retina (Fig. 2a). Consistently, our results showed an increase of CaN immunoreactivity
152 in RNA-binding protein with multiple splicing (RBPMS)-positive RGCs as well as neurons in
153 the inner nuclear layer (INL) of glaucomatous DBA/2J retina (Fig. 2b and c). We also observed
154 a significant increase of total Drp1 protein expression but a significant dephosphorylation of
155 Drp1 Ser637 in glaucomatous DBA/2J retina (Fig. 2d). Consistently, our results showed an

156 increase of Drp1 immunoreactivity in TUJ1-positive RGCs of glaucomatous DBA/2J retina (Fig.
157 2e and f). These results suggest that elevated IOP-induced CaN activation is associated with
158 dephosphorylation of Drp1 at Ser637 in glaucomatous RGCs, leading to mitochondrial fisison[11].
159

160 **Loss of AKAP1 triggers activation of CaN and dephosphorylation of Drp1 at Ser637 in the**
161 **retina**

162 We next used the retinas from mice lacking 10-month-old AKAP1 ($AKAP1^{-/-}$)[24] and age-
163 matched wild-type (WT) mice and examined the expression level of CaN. Following the
164 confirmation of a significant decrease of *AKAP1* gene expression (Fig. 3a), we observed a
165 significant increase of CaN protein expression in $AKAP1^{-/-}$ retina compared with WT retina (Fig.
166 3b). In addition, increased CaN immunoreactivity was present in RBPMS-positive RGCs as well
167 as neurons in the INL in $AKAP1^{-/-}$ retina (Fig. 3c and d). We further examined expression levels
168 of AMP-activated protein kinase (AMPK) and Drp1 protein, as well as phosphorylation of
169 AMPK at threonine 172 (Thr172) and Drp1 at Ser637 in $AKAP1^{-/-}$ retina. There was no
170 significant difference in the phosphorylation of AMPK at Thr172 between WT and $AKAP1^{-/-}$
171 retinas, whereas we observed a significant decrease of total AMPK protein expression in
172 $AKAP1^{-/-}$ retina (Fig. 4a). Interestingly, we observed a significant increase of total Drp1 protein
173 expression in in $AKAP1^{-/-}$ retina (Fig. 4b). Also, $AKAP1^{-/-}$ retina showed a significant
174 dephosphorylation of Drp1at Ser637, whereas there was no significant difference in the
175 phosphorylation of Drp1 at Ser616 between WT and $AKAP1^{-/-}$ retinas (Fig. 4b). Consistent with
176 this finding, increased Drp1 immunoreactivity was present in RBPMS-positive RGCs of
177 $AKAP1^{-/-}$ retina (Fig. 4c and d).
178

179 **AKAP1 loss causes mitochondrial fission and mitophagosome formation in RGCs**

180 We further examined the expression levels of optic atrophy type 1 (OPA1) and mitofusin (Mfn)
181 1 and 2 in $AKAP1^{-/-}$ retina and the alteration of mitochondrial ultrastructure in $AKAP1^{-/-}$ RGC
182 somas. We observed no significant difference in *OPA1* gene expression, but a significant
183 decrease of total OPA1 protein expression in $AKAP1^{-/-}$ retina compared with WT (Fig. 5a).
184 More specifically, small isoform (80 kDa) of OPA1 protein expression was significantly
185 decreased, whereas there was no significant difference in the large isoform (100 kDa) of OPA1
186 protein expression in $AKAP1^{-/-}$ retina (Fig. 5a). We also observed a significant decrease of *Mfn1*

187 gene expression but a significant increase of Mfn1 protein expression, whereas there was no
188 significant difference in Mfn2 protein expression in AKAP1$^{-/-}$ retina (Fig. 5a). Using EM and
189 electron microscope (EM) tomography analyses, we further assessed changes of mitochondrial
190 ultrastructure by measuring mitochondrial volume density, number, cross-sectional area and
191 cristae abundance in AKAP1$^{-/-}$ RGC somas. In comparison with WT mice, representative
192 volumes generated by EM tomography provided evidence for mitochondrial fission and loss of
193 mitochondrial mass (Fig. 5, b-d). Quantitative analysis showed significant decreases of
194 mitochondrial volume density (13 ± 0.7%), and mitochondrial cross-sectional area (0.14 ± 0.02
195 μm^2), but a significant increase of mitochondrial number (0.92 ± 0.06 per μm^2) in AKAP1$^{-/-}$
196 RGC somas compared with WT (22 ± 2 %, mitochondrial volume density; 0.20 ± 0.01 μm^2,
197 mitochondrial cross-sectional area ; 0.67 ± 0.05 per μm^2, mitochondrial number) (Fig. 5c).
198 However, there was no significant difference in mitochondrial cristae abundance, which is the
199 ratio of cristae membrane surface area divided by the mitochondrial outer membrane surface
200 area, between WT and AKAP1$^{-/-}$ RGC somas (Fig. 5c). Using three-dimensional (3D)
201 reconstruction of tomographic volume, we observed that AKAP1$^{-/-}$ mitochondria are
202 significantly smaller than the WT mitochondria. Smaller mitochondria should have fewer
203 cristae, given that cristae shape doesn't change a lot, but the density of cristae was about the same
204 between WT and AKAP1$^{-/-}$ (Fig. 5d). These results suggest that AKAP1 loss induces an
205 imbalance of mitochondrial dynamics by triggering mitochondrial fission and loss in RGCs.
206 AKAP1 loss promotes mitochondrial abnormalities and mitophagy in cardiac injury[46]. Based on
207 our current findings of mitochondrial fission and loss, we determined whether AKAP1 loss
208 induces mitophagosome formation. Indeed, AKAP1 loss significantly enhanced LC3-II protein
209 expression but decreased p62 protein expression in AKAP1$^{-/-}$ retina (Fig. 6a). Our results
210 showed strong LC3 immunoreactivities in RGC somas and axons in the GCL of AKAP1$^{-/-}$ mice
211 (Fig. 6b). Notably, segmented volumes from 3D tomographic reconstructions using EM
212 tomography revealed examples of degraded mitochondria with severe cristae depletion that were
213 engulfed in mitophagosomes in RGC soma of AKAP1$^{-/-}$ mice (Fig. 6c-j).
214
215 **AKAP1 loss results in OXPHOS dysfunction and induces oxidative stress in the retina**
216 Since AKAP1 deletion increased superoxide production in primary hippocampal and cortical
217 neurons in response to glutamate excitotoxicity as well as resulted in OXPHOS complex (Cx) II

218 dysfunction[24], we determined whether loss of AKAP1 alters OXPHOS Cxs and induces
219 oxidative stress in the retina. We further observed that AKAP1 loss significantly increases
220 OXPHOS Cx II but decreased OXPHOS Cx III-V protein expression in AKAP1$^{-/-}$ retina (Fig.
221 7a). However, there was no significant difference in OXPHOS Cx I protein expression between
222 WT and AKAP1$^{-/-}$ retinas (Fig. 7a). We observed a significant increase of superoxide dismutase
223 2 (SOD2) protein expression in AKAP1$^{-/-}$ retina (Fig. 7b). We also observed that SOD2 protein
224 expression was increased in the inner retina, including RGCs in the GCL, of AKAP1$^{-/-}$ mice (Fig.
225 7c and d). These results suggest that AKAP1 loss compromises OXPHOS and may contribute to
226 oxidative stress.
227
228 **AKAP1 loss inactivates Akt and activates Bim/Bax pathway in the retina**
229 We examined the expression levels of Akt protein expression, and Akt phosphorylation at serine
230 473 (Ser473) and threonine 308 (Thr308) in AKAP1$^{-/-}$ retina. We observed a significant increase
231 of total Akt protein expression but a significant dephosphorylation Akt at Ser473 and Thr308
232 protein expression in AKAP1$^{-/-}$ retina (Fig. 8a). Consistently, our results showed that Akt
233 immunoreactivity was increased in the INL and GCL of AKAP1$^{-/-}$ retina (Fig. 8b and c). More
234 specifically, increased Akt immunoreactivity was prominent in Brn3a-positive RGCs of AKAP1^{-}
235 $^{/-}$ mice (Fig. 8b and c). Because Akt inactivation is associated with Bim/Bax activation and
236 intrinsic apoptotic cell death[47,48], we further determined whether AKAP1 loss activates Bim/Bax
237 in the retina. We observed significant increases of Bim and Bax protein expression in AKAP1$^{-/-}$
238 retina (Fig. 8d). In addition, we observed that Bax immunoreactivity was increased in the GCL
239 of AKAP1$^{-/-}$ retina (Fig. 8d). More specifically, increased Bax immunoreactivity was prominent
240 in RBPMS-positive RGCs of AKAP1$^{-/-}$ mice (Fig. 8e and f).
241
242
243
244
245
246
247
248

249 **Discussion**

250 We here demonstrated for the first time that RGCs showed AKAP1 immunoreactivity in D2-
251 *Gpnmb*+ mice and elevated IOP triggered loss of AKAP1 in glaucomatous RGCs. In addition,
252 elevated IOP increased CaN and total Drp1 levels in glaucomatous RGCs. It also impaired Drp1
253 phosphorylation at Ser637 in glaucomatous retina. These results suggest that AKAP1 and Drp1
254 phosphorylation at Ser637 have critical roles in RGC mitochondria and survival against
255 glaucomatous damage. We also observed that loss of AKAP1 increased CaN and total Drp1
256 levels in RGCs, and compromised Drp1 phosphorylation at Ser637 in the retina, leading to
257 mitochondrial fission and loss, and mitophagosome formation in RGCs. In addition, loss of
258 AKAP1 resulted in OXPHOS dysfunction, as well as Akt inactivation and Bim/Bax activation;
259 these effects contribute to glaucomatous neurodegeneration.

260 Impairment of mitochondrial dynamics is critically involved in glaucomatous RGCs and
261 their axon degeneration[8,9,11,36], and inhibition of Drp1 rescues RGCs and their axons by
262 preserving mitochondrial integrity in experimental glaucoma[11,36]. Our previous study
263 demonstrated that elevated IOP showed a significant increase of total Drp1 level, while it did not
264 alter phosphorylation of Drp1 at Ser616 in glaucomatous retina[11]; these effects suggest that
265 elevated IOP-mediated mitochondrial fission activity is not dependent on Drp1 phosphorylation
266 at Ser616 in glaucomatous RGC degeneration. Hence, our novel finding that glaucomatous
267 RGCs lacking AKAP1 trigger CaN-mediated dephosphorylation of Drp1 at Ser637 suggest an
268 important rationale to further investigate the impact of AKAP1 loss, mitochondrial fission and its
269 related signaling pathway in RGCs.

270 AKAP1 is an important regulator of mitochondrial function by PKA anchoring and Drp1
271 phosphorylation at Ser637, and overexpression of AKAP1 is neuroprotective in neuronal cells
272 against the mitochondrial toxin rotenone[20,21,23,24,43]. Emerging evidence showed that mice
273 lacking AKAP1 exhibit increased infarct following transient cerebral ischemia as well as
274 increased Drp1 localization to mitochondria from the forebrain tissues and decreased Drp1
275 phosphorylation at Ser637[24]. Our findings of enhanced CaN-mediated Drp1 phosphorylation at
276 Ser637, and extensive mitochondrial fission and loss in the retina of AKAP1$^{-/-}$ mice suggest that
277 AKAP1 loss directly contributes to Drp1 phosphorylation-dependent mitochondrial fission and
278 loss in glaucomatous RGCs. This notion is also supported by the evidence of increasing LC3-II
279 and decreasing p62 levels, as well as mitophagosome formation that contains degrading

280 mitochondria in RGC somas of AKAP1$^{-/-}$ mice. In addition, it is supported by the evidence of
281 our previous report showing autophagosome/mitophagosome formation in RGC axons of
282 glaucomatous DBA/2J mice[11].
283 AMPK is a nutrient and energy sensor that maintains energy homeostatsis[49] and mediates
284 mitochondrial fission in response to energy stress[50]. It has been reported that there was evidence
285 of AMPK activation by increasing AMPK phosphorylation at Thr172 in the retina and optic
286 nerve in glaucomatous DBA/2J mice[14,51]. Also, it has been proposed that AMPK uncouples
287 PKA from D-AKAP1 (AKAP140/149 and other splice variants AKAP121, sAKAP84) to
288 promote mitochondrial fission and mitophagy[52]. Furthermore, AMPK is associated with the
289 regulation of Drp1 phosphorylation[53,54]. In the current study, our findings showed no significant
290 evidence of AMPK activation, suggesting that AKAP1 loss may not directly contribute to
291 AMPK activation in the retina. Because energy stress activates AMPK[14,55], it is also possible
292 that AKAP1 loss may not trigger an excessive energy stress and substantial energy deficit in the
293 retina. In the line of this notion, our results showed that the level of dephosphorylation of Drp1
294 Ser637 in AKAP1$^{-/-}$ retina was relatively modest compared to the level of dephosphorylation of
295 Drp1 Ser637 in glaucomatous retina. Hence, our results intriguingly raise a possibility that
296 combined induction of both AMPK activation and AKAP1 loss may exacerbate mitochondrial
297 fission and loss in glaucomatous RGCs and their axons, leading to the promotion of energy crisis
298 and cell death. We believe that further studies will be required to investigate the relationship
299 between AMPK activation and AKAP1 loss in glaucomatous RGCs.
300 The increase in LC3-II accumulates autophagosomes, but does not guarantee autophagic
301 degradation. If, however, the amount of LC3-II further accumulates in the presence of lysosomal
302 protease inhibitors, this would indicate enhancement of autophagic flux[56]. On the other hand, the
303 protein expression level of p62/SQSTM1, a polyubiquitin binding protein, serves as autophagic
304 receptor and is a good indicator of autophagic flux[57-59]. Also, p62 protein expression has been
305 used as autophagic marker with LC3-II[60]. Although p62 level alone is not indicative of
306 activation of autophagy, p62 is also a marker for the degradation phase of autophagosomes and
307 has a lot of functions beyond autophagy[59]. In the current study, our findings showed that loss of
308 AKAP1 increased LC3-II protein expression but decreased p62 protein expression in AKAP1$^{-/-}$
309 retina. Intriguingly, AKAP1$^{-/-}$ heart reduced p62 protein expression and enhanced mitophagy and
310 apoptosis[46]. Collectively, our results suggest that the increased LC3-II and decreased p62

311 contribute to the induction of autophagy/mitophagy in AKAP1$^{-/-}$ retina. Hence, we raise a
312 possibility that loss of AKAP1 may not only induce autophagosome/mitophagosome formation,
313 but also trigger increase of autophagic flux and degradation in RGCs. Also, whether this
314 autophagic/mitophagic process is a compensatory or pathological pathway in AKAP1$^{-/-}$ retina
315 should be considered in the future studies.
316 Previous study indicated the notion that AKAP1 regulates mitochondrial dynamics by
317 posttranslational modifications, but levels of Drp1, OPA1 and Mfn2 were unaltered in total
318 forebrain homogenates from AKAP1$^{-/-}$ mice[24]. Of interest, however, we observed a decrease of
319 total OPA1, but an increase of total Drp1 and Mfn1 in the retina of AKAP1$^{-/-}$ mice. Inner
320 membrane-anchored long OPA1 (L-OPA1) undergoes proteolytic cleavage resulting in short
321 OPA1 (S-OPA1)[61]. Cells contain a mixture of L-OPA1, required for mitochondrial fusion and S-
322 OPA, which facilitate mitochondrial fission under normal conditions. Disruption of this balance
323 in times of stress, result in mitochondrial fragmentation[61]. Thus, these unexpected, but important
324 results propose the possibility that AKAP1 may contribute to the regulation of mitochondrial
325 dynamics not only by posttranslational modifications, but also by alteration of fusion/fission
326 protein expression in the retina. Future studies will be needed to clarify the molecular
327 mechanisms underlying the alteration of fusion/fission proteins in the retina lacking AKAP1.
328 Emerging evidence showed that AKAP1 deletion results in OXPHOS Cx II dysfunction
329 in neuronal cells[24]. OXPHOS Cx II is a source of the mitochondrial reserve respiratory capacity
330 that is regulated by metabolic sensor and promotes cell survival against hypoxia. In the present
331 study, the observation that increasing OXPHOS Cx II, but decreasing OXPHOS Cxs III-V
332 activities triggered by loss of AKAP1 in the retina is likely to imply that AKAP1 plays a critical
333 role in OXPHOS function in RGCs. Moreover, increasing OXPHOS Cx II activity may be an
334 important endogenous compensatory defense mechanism in response to oxidative stress.
335 Further, this imbalance of OXPHOS Cxs suggests another possibility that AKAP1 loss may
336 contribute to an increase of ROS production and decrease of ATP production in the retina that
337 are previously reported in pressure and/or oxidative stress-induced RGC degeneration[11]. In
338 particular, association of POAG with polymorphism of mitochondrial cytochrome c oxidase
339 subunit 1 of OXPHOS Cx IV suggests a potential role of abnormal OXPHOS-mediated
340 mitochondrial dysfunction in glaucoma pathogenesis[3,4]. Therefore, these results collectively
341 suggest that AKAP1 loss in glaucomatous retina contributes to OXPHOS dysfunction that is

342 associated with metabolic and oxidative stress by increasing ROS production and decreasing
343 ATP reduction, leading to RGC death during glaucomatous neurodegeneration.
344 Loss of AKAP1 inactivates Akt signaling and increases apoptosis in cardiac
345 dysfunction[62,63]. Akt pathway controls the expression of apoptosis-related gene through
346 transcription factors such as FoxO (FoxO1 and FoxO3a)[64,65] and Akt activation promotes cell
347 survival by inhibiting FoxO3a/Bim/Bax pathway[48,64,65]. The pro-apoptotic Bcl-2 homology
348 domain 3-only protein Bim induces apoptosis, primarily through its increased binding activity
349 toward multiple pro-survival Bcl-2-like proteins, whose dissociations activate Bak and Bax[66,67].
350 In addition, Bax-mediated mitochondrial outer membrane permeabilization is an important
351 pathophysiological mechanism for metabolic dysfunction and cell death[68,69], and Bax activation
352 plays a critical role in mitochondrial dysfunction-mediated RGC degeneration[11,12]. Because
353 Drp1 contributes to Bax oligomerization, mitochondrial fission and the cellular apoptotic
354 pathway[70-72], increased total Drp1 and Bax levels in AKAP1$^{-/-}$ retinas suggest that AKAP1 loss
355 may contribute to Drp1-mediated Bax oligomerization, leading to mitochondrial fission. Recent
356 evidence from our group and others indicated that activation of cAMP/PKA pathway promotes
357 RGC survival [48,73-75] and that AKAP1-mediated neuroprotection requires PKA anchoring and
358 Drp1 phosphorylation at Ser637[21,23,24,43,76]. In this regard, our observation that AKAP1$^{-/-}$ retinas
359 dephosphorylates Akt at Ser473 and SerT308, and activates Bim/Bax pathway raise the
360 possibility that AKAP1 may be critical to RGC protection by modulating Akt/Bim/Bax pathway
361 against glaucomatous damage. Future studies will be necessary to examine whether
362 overexpression of AKAP1 rescues RGCs by promoting Drp1 phosphorylation at S637,
363 maintaining metabolic activity, activating Akt pathway and inhibiting Bim/Bax pathway.
364 In summary, our results represent the first direct evidence of a Drp1 phosphorylation-
365 mediated mitochondrial pathogenic mechanism that leads to mitochondrial fission and metabolic
366 dysfunction in glaucomatous RGC degeneration. Also, we provide evidence for the first time that
367 AKAP1 loss-mediated CaN activation and Drp1 dephosphorylation at Ser637 result in
368 mitochondrial fission, mitophagosome formation, OXPHOS dysfunction and oxidative stress, as
369 well as Akt inactivation and Bim/Bax activation in RGCs. Therefore, we propose
370 overexpression of AKAP1 and modulation of Drp1 phosphorylation at Ser637 as therapeutic
371 strategies for neuroprotective intervention in glaucoma and other mitochondria-related optic
372 neuropathies.

373 **Materials and methods**

374 **Animals**

375 Adult female DBA/2J and D2-*Gpnmb*$^{+}$ mice (The Jackson Laboratory), and adult male WT and
376 AKPA1$^{-/-}$ mice were housed in covered cages, fed with a standard rodent diet ad libitum, and
377 kept on a12 h light/12 h dark cycle. Animals were assigned randomly to experimental and
378 control groups. The following PCR primers were used to determine AKAP1 genotype:
379 GGAGGCGATCACAGCAACAACCG (R), ATACAGAAGCAGATCACTCAGGAGG (F-
380 WT), CAGTCCCAAGGCTCATTTCAGGCC (F-KO)[24]. To investigate the effect of IOP
381 elevation, 20 10 month-old DBA/2J and 10 age-matched D2-*Gpnmb*$^{+}$ mice were used. To
382 investigate the effect of AKAP1 loss, 10 10 month-old AKAP1$^{-/-}$ and 10 age-matched WT mice
383 were used. All procedures concerning animals were in accordance with the Association for
384 Research in Vision and Ophthalmology Statement for the Use of Animals in Ophthalmic Vision
385 Research and under protocols approved by Institutional Animal Care and Use Committee at the
386 University of California, San Diego.

387

388 **Tissue preparation**

389 Mice were anesthetized by an intraperitoneal (IP) injection of a cocktail of ketamine (100 mg/kg,
390 Ketaset; Fort Dodge Animal Health) and xylazine (9 mg/kg, TranquiVed; VEDCO Inc.) prior to
391 cervical dislocation. The investigators were not blinded during tissue and data collection from
392 mice. Blinding was used during data analysis. For immunohistochemistry, the retinas were
393 dissected from the choroids and fixed with 4% paraformaldehyde (Sigma-Aldrich) in phosphate
394 buffered saline (PBS, pH 7.4) for 2 h at 4 °C. Retinas were washed several times with PBS then
395 dehydrated through graded levels of ethanol and embedded in polyester wax. For Western blot
396 and PCR analyses, extracted retinas were immediately used.

397

398 **Western blot analyses**

399 Harvested retinas (n = 4 retinas/group) were homogenized for 1 min on ice with a modified
400 RIPA lysis buffer (150 mM NaCl, 1 mM EDTA, 1% NP-40, 0.1% SDS, 1 mM DTT, 0.5%
401 sodium deoxycholate and 50 mM Tris-Cl, pH 7.6), containing complete protease inhibitors. The
402 lysates were then centrifuged at 15,000 g for 15 min and protein amounts in the supernatants
403 were measured by Bradford assay. Proteins (10-20 μg) were separated by SDS/PAGE and

404 electrotransferred to polyvinylidene difluoride membranes (GE Healthcare Bio-Science). The
405 membranes were blocked with 5% non-fat dry milk and PBS/0.1% Tween-20 (PBS-T) for 1 h at
406 room temperature and incubated with primary antibodies for overnight at 4 °C. Primary
407 antibodies are mouse monoclonal anti-Actin antibody (1:20,000; Millipore; Cat#, MAB1501),
408 rabbit monoclonal anti-AKAP1 (1:1000; Cell Signaling; Cat# 5203), rabbit polyclonal anti-Akt
409 antibody (1:5000; Cell Signaling; Cat# 92725), mouse monoclonal anti-phospho-Akt Ser473
410 antibody (1:100, Cell Signaling; Cat# 9271), rabbit monoclonal anti-phospho-Akt Thr308
411 antibody (1:1000, Cell Signaling; Cat# 4056), rabbit polyclonal anti-AMPKα1/2 antibody
412 (1:1000, Santa Cruz Biotechnology; Cat# sc25792), rabbit monoclonal anti-AMPKα Thr172
413 antibody (1:1000, Cell Signaling Cat# 2535), mouse monoclonal anti-Bax antibody (6A7; 1:500;
414 Santa Cruz Biotechnology; Cat# sc-23959), rabbit polyclonal anti-Bim antibody (1:100, Santa
415 Cruz Biotechnology; Cat# sc-8265), mouse monoclonal anti-CaN antibody (1:200, BD
416 Bioscience; Cat# 610259), mouse monoclonal anti-Drp1 antibody (1:1000; BD Biosciences;
417 Cat# 611113), rabbit polyclonal phospho-Drp1 Ser637 antibody (1:750; Cell Signaling; Cat#
418 4867), rabbit polyclonal phospho-Drp1 Ser616 antibody (1:750; Cell Signaling; Cat# 3455),
419 rabbit polyclonal anti-LC3 antibody (1:2000; MBL International; Cat# PM036), mouse
420 monoclonal anti-Mfn1 antibody (1:20000; Abcam; Cat# ab57602), mouse monoclonal anti-Mfn2
421 antibody (1:2000; Abcam; Cat# ab56889), mouse monoclonal anti-OPA1 antibody (1:2000; BD
422 Biosciences; Cat# 612607), rat/mouse monoclonal anti-OXPHOS Cx Cocktail Kit (1:1000;
423 Invitrogen; Cat# 458099), rabbit polyclonal p62 antibody (1:1000; MBL International; Cat#
424 PM045) and rabbit polyclonal anti-SOD2 antibody (1:5000; Santa Cruz; Cat# sc-30080).
425 Membrane were washed several times with PBS-T then incubated with peroxidase-conjugated
426 goat anti-mouse or rabbit IgG (1:1000-7000; Bio-Rad; Cat# 1721011 or 1706515) for 1 h at
427 room temperature and developed using enhanced chemiluminescence substrate system. The
428 images were captured and quantified by using ImageQuant™ LAS 4000 system (GE Healthcare
429 Bio-Science) and band densities were normalized to that of actin, total Drp1, total Akt, or total
430 AMPK.
431
432 **Immunohistochemistry**
433 Immunohistochemical staining of 7 μm wax sections of full thickness retina were performed.
434 Sections from wax blocks from each group (n = 4 retinas/group) were used for

435 immunohistochemical analysis. Primary antibodies included rabbit monoclonal anti-AKAP1
436 antibody (1:100, Cell Signaling; Cat# 5203), rabbit polyclonal anti-Akt antibody (1:100, Cell
437 Signaling; Cat# 92725), mouse monoclonal anti-Bax antibody (6A7; 1:50, Santa Cruz
438 Biotechnology; Cat# sc-23959), goat polyclonal anti-Brn3a antibody (1:500, Santa Cruz
439 Biotechnology; Cat# sc-23959), mouse monoclonal anti-CaN (1:200, BD Bioscience; Cat#
440 610259), mouse monoclonal anti-Drp1 antibody (1:25; BD Biosciences; Cat# 611113), rabbit
441 polyclonal anti-Drp1 (1:50, Santa Cruz Biotechnology, Cat# sc-32898), rabbit polyclonal anti-
442 LC3 antibody (1:2000; MBL International) ; Cat# PM036, rabbit polyclonal anti-RBPMS (1:300,
443 Novus; Cat# NBP2-20112), rabbit polyclonal anti-SOD2 antibody (1:300, Santa Cruz
444 Biotechnology; Cat# sc-30080) and mouse monoclonal anti-TUJ1 (1:300, BioLegend; Ct#
445 801202). To prevent non-specific background, tissues were incubated in 1% bovine serum
446 albumin/PBS for 1 h at room temperature before incubation with the primary antibodies for 16 h
447 at 4°C. After several wash steps, the tissues were incubated with the secondary antibodies,
448 Alexa Fluor 488 or 568 dye-conjugated donkey anti-mouse IgG (1:100, Invitrogen; Cat# R37114
449 or A10037), Alexa Fluor 488 or 568 dye-conjugated donkey anti-rabbit IgG (1:100, Invitrogen;
450 Cat# R37118 or A10042) and Alexa Fluor 568 dye-conjugated donkey anti-goat IgG (1:100,
451 Invitrogen; Cat# A11057) for 4 h at 4°C and subsequently washed with PBS. The sections were
452 counterstained with the nucleic acid stain Hoechst 33342 (1 μg/mL; Invitrogen) in PBS. Images
453 were acquired with confocal microscopy (Olympus FluoView1000; Olympus, Tokyo, Japan).
454 Each target protein fluorescent integrated intensity in pixel per area was measured using the
455 ImageJ software[77-79]. All imaging parameters was remained the same and corrected with the
456 background subtraction.
457
458 **RT-PCR and quantitative real-time RT-PCR**
459 Total RNA was isolated from retinas of each group (n = 4 retinas/group) using the Absolutely
460 RNA Miniprep Kit (Stratagene), according to the manufacturer's protocol as previously
461 described[48]. cDNAs were synthesized from total RNAs with iScript cDNA Synthesis Kit (Bio-
462 Rad) according to the manufacturer's protocols. Reverse Transcription (RT)-PCR was
463 performed with cDNAs synthesized from 1 μg of the total RNA of each group as a template and
464 specific primers for: AKAP1, CTGCCAGTCAGTACTCAGCC (F),
465 CTTTGGCACCTCGATCTCCC (R), OPA1, CATCTACCTTCCAGCTGCCC (F),

466 TCTCCTCCTTCACAGCCTCC (R), and Mfn1, GTTTTCCCTGGGCTGGTCTT (F),
467 TTTTCCAAATCACGCCCCCA (R). For the quantification of the relative mRNA expressions
468 of each group, real-time PCR was carried out using MX3000P real-time PCR system
469 (Stratagene) as follows. cDNAs were amplified using SSO Adv. Universal SYBR Green
470 SuperMix (Bio-Rad) and the specific primers for 40 cycles (95 °C for 5 min, and 40 cycles
471 (95 °C for 30 sec, 60 °C for 30 sec, and 72 °C for 30 sec)). Output data were obtained
472 as *Ct* values and the differential mRNA expression of the target genes among groups was
473 calculated using the comparative *Ct* method. GAPDH mRNA, an internal control, was amplified
474 along with the target gene, and the *Ct* value of GAPDH was used to normalize the expression of
475 the target gene.
476
477 **Transmission electron microscopy**
478 For conventional EM, two eyes from each group (n = 2 mice) were fixed via cardiac perfusion
479 with 2% paraformaldehyde, 2.5% glutaraldehyde (Ted Pella, Redding, CA) in 0.15M sodium
480 cacodylate (pH 7.4, Sigma) solution at 37°C and placed in pre-cooled fixative of the same
481 composition on ice for 1 h. The following procedure was used to optimize mitochondrial
482 structural preservation and membrane contrast. The retinas were dissected in a solution of
483 0.15M sodium cacodylate plus 3mM calcium chloride (pH 7.4) on ice and then post-fixed with a
484 1% osmium tetroxide, 0.8% potassium ferrocyanide, 3mM calcium chloride in 0.1M sodium
485 cacodylate solution (pH 7.4) for 1 h, washed with ice-cold distilled water, poststained with 2%
486 uranyl acetate solution at 4°C, dehydrated using graded ethanols, and embedded in Durcupan
487 resin (Fluka). A similar procedure was used for cultured primary RGCs from each group.
488 Ultrathin (70 nm) sections were post-stained with uranyl acetate and lead salt solutions and
489 evaluated using a JEOL 1200FX transmission EM operated at 80kV. Images were recorded on
490 film at 8,000X magnification. The negatives were digitized at 1800 dpi using a Nikon Cool scan
491 system, giving an image size of 4033 x 6010 pixel array and a pixel resolution of 1.77 nm. For
492 quantitative analysis, the number of mitochondria was normalized to the total area occupied by
493 axons in each image, which was measured using ImageJ (http://rsb.info.nih.gov/ij/).
494 Mitochondrial lengths were measured with ImageJ. The mitochondrial volume density, defined
495 as the volume occupied by mitochondria divided by the volume occupied by the axoplasm, was
496 estimated using stereology as follows. A 112 x 112 square grid (112 x 112 chosen for ease of use

497 with Photoshop) was overlaid on each image loaded in Photoshop (Adobe Systems Inc.), and
498 mitochondria and axoplasm lying under intercepts were counted. The relative volume of
499 mitochondria was expressed as the ratio of intercepts coinciding with this organelle relative to
500 the intercepts coinciding with axoplasm.
501
502 **Electron microscope tomography**
503 Sections of retina tissues from each group were cut at a thickness of 400 nm. For each
504 reconstruction, a double-tilt series of images at one degree tilt increment was collected with an
505 FEI titan hibase electron microscope operated at 300 kV. Images were recorded with a Gatan
506 4Kx4K CCD camera. The magnification was 11,000x and the pixel resolution was 0.81 nm.
507 The IMOD package was used for alignment, reconstruction and volume segmentation. Volume
508 segmentation was performed by manual tracing of membranes in the planes of highest resolution
509 with the Drawing Tools and Interpolator plug-ins[80]. The mitochondrial reconstructions and
510 surface-rendered volumes were visualized using 3DIMOD. Measurements of mitochondrial
511 outer, inner boundary, and cristae membrane surface areas and volumes were made within
512 segmented volumes using IMODinfo. These were used to determine the cristae abundance,
513 defined as the ratio: sum of the cristae membrane surface areas divided by the mitochondrial
514 outer membrane surface area. Movies of the tomographic volume were made using IMODmovie.
515
516 **Statistical analyses**
517 Data were shown as mean ± S.D. Comparison of experimental conditions was evaluated using
518 the two-tailed unpaired Student's t-test between groups. $P < 0.05$ was considered to be
519 statistically significant.
520
521
522
523
524
525
526
527

Acknowledgements

This work was supported, in part, by NIH grants EY018658, P30 EY022589, T32 EY026590, 5P41GM103412, and an unrestricted grant from Research to Prevent Blindness (New York, NY) and UCSD Academic Senate.

Conflict of Interest

The authors declare no conflict of interest.

558 **References**

559 1 Weinreb, R. N. & Khaw, P. T. Primary open-angle glaucoma. *Lancet* **363**, 1711-1720
560 (2004).
561
562 2 Abu-Amero, K. K. & Bosley, T. M. Mitochondrial abnormalities in patients with LHON-
563 like optic neuropathies. *Invest Ophthalmol Vis Sci* **47**, 4211-4220 (2006).
564
565 3 Collins, D. W. *et al.* The MT-CO1 V83I Polymorphism is a Risk Factor for Primary
566 Open-Angle Glaucoma in African American Men. *Invest Ophthalmol Vis Sci* **59**, 1751-
567 1759 (2018).
568
569 4 Collins, D. W. *et al.* Association of primary open-angle glaucoma with mitochondrial
570 variants and haplogroups common in African Americans. *Mol Vis* **22**, 454-471 (2016).
571
572 5 Bosley, T. M. *et al.* Down-regulation of OPA1 in patients with primary open angle
573 glaucoma. *Mol Vis* **17**, 1074-1079 (2011).
574
575 6 Lee, S. *et al.* Impaired complex-I-linked respiration and ATP synthesis in primary open-
576 angle glaucoma patient lymphoblasts. *Invest Ophthalmol Vis Sci* **53**, 2431-2437 (2012).
577
578 7 Singh, L. N. *et al.* Mitochondrial DNA Variation and Disease Susceptibility in Primary
579 Open-Angle Glaucoma. *Invest Ophthalmol Vis Sci* **59**, 4598-4602 (2018).
580
581 8 Ju, W. K. *et al.* Intraocular pressure elevation induces mitochondrial fission and triggers
582 OPA1 release in glaucomatous optic nerve. *Invest Ophthalmol Vis Sci* **49**, 4903-4911
583 (2008).
584
585 9 Ju, W. K. *et al.* Increased optic atrophy type 1 expression protects retinal ganglion cells
586 in a mouse model of glaucoma. *Mol Vis* **16**, 1331-1342 (2010).
587
588 10 Lee, D. *et al.* Coenzyme Q10 inhibits glutamate excitotoxicity and oxidative stress-
589 mediated mitochondrial alteration in a mouse model of glaucoma. *Invest Ophthalmol Vis*
590 *Sci* **55**, 993-1005 (2014).
591
592 11 Kim, K. Y. *et al.* DRP1 inhibition rescues retinal ganglion cells and their axons by
593 preserving mitochondrial integrity in a mouse model of glaucoma. *Cell Death Dis* **6**,
594 e1839 (2015).
595
596 12 Shim, M. S. *et al.* Mitochondrial pathogenic mechanism and degradation in optineurin
597 E50K mutation-mediated retinal ganglion cell degeneration. *Sci Rep* **6**, 33830 (2016).
598
599 13 Williams, P. A. *et al.* Vitamin B3 modulates mitochondrial vulnerability and prevents
600 glaucoma in aged mice. *Science* **355**, 756-760 (2017).
601

602 14 Harun-Or-Rashid, M. *et al.* Structural and Functional Rescue of Chronic Metabolically
603 Stressed Optic Nerves through Respiration. *J Neurosci* **38**, 5122-5139 (2018).
604
605 15 Herberg, F. W., Maleszka, A., Eide, T., Vossebein, L. & Tasken, K. Analysis of A-kinase
606 anchoring protein (AKAP) interaction with protein kinase A (PKA) regulatory subunits:
607 PKA isoform specificity in AKAP binding. *J Mol Biol* **298**, 329-339 (2000).
608
609 16 Affaitati, A. *et al.* Essential role of A-kinase anchor protein 121 for cAMP signaling to
610 mitochondria. *J Biol Chem* **278**, 4286-4294, doi:10.1074/jbc.M209941200 (2003).
611 17 Rubin, C. S. A kinase anchor proteins and the intracellular targeting of signals carried by
612 cyclic AMP. *Biochim Biophys Acta* **1224**, 467-479 (1994).
613
614 18 Colledge, M. & Scott, J. D. AKAPs: from structure to function. *Trends Cell Biol* **9**, 216-
615 221 (1999).
616
617 19 Huang, L. J., Durick, K., Weiner, J. A., Chun, J. & Taylor, S. S. D-AKAP2, a novel
618 protein kinase A anchoring protein with a putative RGS domain. *Proc Natl Acad Sci U S*
619 *A* **94**, 11184-11189 (1997).
620
621 20 Merrill, R. A. & Strack, S. Mitochondria: a kinase anchoring protein 1, a signaling
622 platform for mitochondrial form and function. *Int J Biochem Cell Biol* **48**, 92-96 (2014).
623
624 21 Dickey, A. S. & Strack, S. PKA/AKAP1 and PP2A/Bbeta2 regulate neuronal
625 morphogenesis via Drp1 phosphorylation and mitochondrial bioenergetics. *J Neurosci*
626 **31**, 15716-15726 (2011).
627
628 22 Gomes, L. C., Di Benedetto, G. & Scorrano, L. During autophagy mitochondria elongate,
629 are spared from degradation and sustain cell viability. *Nat Cell Biol* **13**, 589-598 (2011).
630
631 23 Merrill, R. A. *et al.* Mechanism of neuroprotective mitochondrial remodeling by
632 PKA/AKAP1. *PLoS Biol* **9**, e1000612 (2011).
633
634 24 Flippo, K. H. *et al.* AKAP1 Protects from Cerebral Ischemic Stroke by Inhibiting Drp1-
635 Dependent Mitochondrial Fission. *J Neurosci* **38**, 8233-8242 (2018).
636
637 25 Knott, A. B., Perkins, G., Schwarzenbacher, R. & Bossy-Wetzel, E. Mitochondrial
638 fragmentation in neurodegeneration. *Nat Rev Neurosci* **9**, 505-518 (2008).
639
640 26 Burte, F., Carelli, V., Chinnery, P. F. & Yu-Wai-Man, P. Disturbed mitochondrial
641 dynamics and neurodegenerative disorders. *Nat Rev Neurol* **11**, 11-24 (2015).
642
643 27 Chen, H. & Chan, D. C. Emerging functions of mammalian mitochondrial fusion and
644 fission. *Hum Mol Genet* **14 Spec No. 2**, R283-289 (2005).
645
646 28 Okamoto, K. & Shaw, J. M. Mitochondrial morphology and dynamics in yeast and
647 multicellular eukaryotes. *Annu Rev Genet* **39**, 503-536 (2005).

29 Cho, D. H. *et al.* S-nitrosylation of Drp1 mediates beta-amyloid-related mitochondrial fission and neuronal injury. *Science* **324**, 102-105 (2009).

30 Kim, J. *et al.* Mitochondrial loss, dysfunction and altered dynamics in Huntington's disease. *Hum Mol Genet* **19**, 3919-3935 (2010).

31 Song, W. *et al.* Mutant huntingtin binds the mitochondrial fission GTPase dynamin-related protein-1 and increases its enzymatic activity. *Nat Med* **17**, 377-382 (2011).

32 Dowding, J. M. *et al.* Cerium oxide nanoparticles protect against Abeta-induced mitochondrial fragmentation and neuronal cell death. *Cell death and differentiation* **21**, 1622-1632 (2014).

33 Cereghetti, G. M. *et al.* Dephosphorylation by calcineurin regulates translocation of Drp1 to mitochondria. *Proc Natl Acad Sci U S A* **105**, 15803-15808 (2008).

34 Cribbs, J. T. & Strack, S. Reversible phosphorylation of Drp1 by cyclic AMP-dependent protein kinase and calcineurin regulates mitochondrial fission and cell death. *EMBO Rep* **8**, 939-944 (2007).

35 Chang, C. R. & Blackstone, C. Cyclic AMP-dependent protein kinase phosphorylation of Drp1 regulates its GTPase activity and mitochondrial morphology. *The Journal of biological chemistry* **282**, 21583-21587 (2007).

36 Park, S. W. *et al.* A selective inhibitor of drp1, mdivi-1, increases retinal ganglion cell survival in acute ischemic mouse retina. *Invest Ophthalmol Vis Sci* **52**, 2837-2843 (2011).

37 Ju, W. K. *et al.* Elevated hydrostatic pressure triggers mitochondrial fission and decreases cellular ATP in differentiated RGC-5 cells. *Invest Ophthalmol Vis Sci* **48**, 2145-2151 (2007).

38 John, S. W., Hagaman, J. R., MacTaggart, T. E., Peng, L. & Smithes, O. Intraocular pressure in inbred mouse strains. *Invest Ophthalmol Vis Sci* **38**, 249-253 (1997).

39 Libby, R. T. *et al.* Inherited glaucoma in DBA/2J mice: pertinent disease features for studying the neurodegeneration. *Vis Neurosci* **22**, 637-648 (2005).

40 Libby, R. T. *et al.* Susceptibility to neurodegeneration in a glaucoma is modified by Bax gene dosage. *PLoS Genet* **1**, 17-26 (2005).

41 Abrenica, B., AlShaaban, M. & Czubryt, M. P. The A-kinase anchor protein AKAP121 is a negative regulator of cardiomyocyte hypertrophy. *J Mol Cell Cardiol* **46**, 674-681 (2009).

42 Rogne, M., Stokka, A. J., Tasken, K., Collas, P. & Kuntziger, T. Mutually exclusive binding of PP1 and RNA to AKAP149 affects the mitochondrial network. *Hum Mol Genet* **18**, 978-987 (2009).

694 43 Dagda, R. K. *et al.* Mitochondrially localized PKA reverses mitochondrial pathology and
695 dysfunction in a cellular model of Parkinson's disease. *Cell Death Differ* **18**, 1914-1923
696 (2011).
697
698 44 Kim, H. *et al.* Fine-tuning of Drp1/Fis1 availability by AKAP121/Siah2 regulates
699 mitochondrial adaptation to hypoxia. *Mol Cell* **44**, 532-544 (2011).
700
701 45 Huang, W. *et al.* Calcineurin cleavage is triggered by elevated intraocular pressure, and
702 calcineurin inhibition blocks retinal ganglion cell death in experimental glaucoma. *Proc*
703 *Natl Acad Sci U S A* **102**, 12242-12247 (2005).
704
705 46 Schiattarella, G. G. *et al.* Akap1 Deficiency Promotes Mitochondrial Aberrations and
706 Exacerbates Cardiac Injury Following Permanent Coronary Ligation via Enhanced
707 Mitophagy and Apoptosis. *PLoS One* **11**, e0154076 (2016).
708
709 47 Kong, D. *et al.* Insulin-like growth factor 1 rescues R28 retinal neurons from apoptotic
710 death through ERK-mediated BimEL phosphorylation independent of Akt. *Exp Eye Res*
711 **151**, 82-95 (2016).
712
713 48 Shim, M. S. *et al.* Elevated intracellular cAMP exacerbates vulnerability to oxidative
714 stress in optic nerve head astrocytes. *Cell Death Dis* **9**, 285 (2018).
715
716 49 Hardie, D. G., Ross, F. A. & Hawley, S. A. AMPK: a nutrient and energy sensor that
717 maintains energy homeostasis. *Nat Rev Mol Cell Biol* **13**, 251-262 (2012).
718
719 50 Toyama, E. Q. *et al.* Metabolism. AMP-activated protein kinase mediates mitochondrial
720 fission in response to energy stress. *Science* **351**, 275-281 (2016).
721
722 51 Harun-Or-Rashid, M. & Inman, D. M. Reduced AMPK activation and increased HCAR
723 activation drive anti-inflammatory response and neuroprotection in glaucoma. *J*
724 *Neuroinflammation* **15**, 313 (2018).
725
726 52 Zhang, J., Wang, Y., Liu, X., Dagda, R. K. & Zhang, Y. How AMPK and PKA Interplay
727 to Regulate Mitochondrial Function and Survival in Models of Ischemia and Diabetes.
728 *Oxid Med Cell Longev* **2017**, 4353510 (2017).
729
730 53 Li, J. *et al.* Pharmacological activation of AMPK prevents Drp1-mediated mitochondrial
731 fission and alleviates endoplasmic reticulum stress-associated endothelial dysfunction. *J*
732 *Mol Cell Cardiol* **86**, 62-74 (2015).
733
734 54 Zhou, H. *et al.* Empagliflozin rescues diabetic myocardial microvascular injury via
735 AMPK-mediated inhibition of mitochondrial fission. *Redox Biol* **15**, 335-346 (2018).
736
737 55 Garcia, D. & Shaw, R. J. AMPK: Mechanisms of Cellular Energy Sensing and
738 Restoration of Metabolic Balance. *Mol Cell* **66**, 789-800 (2017).

739 56 Mizushima, N. & Yoshimori, T. How to interpret LC3 immunoblotting. *Autophagy* **3**,
740 542-545 (2007).
741
742 57 Shin, J. P62 and the sequestosome, a novel mechanism for protein metabolism. *Arch*
743 *Pharm Res* **21**, 629-633 (1998).
744
745 58 Bitto, A. *et al.* P62/SQSTM1 at the interface of aging, autophagy, and disease. *Age*
746 *(Dordr)* **36**, 9626 (2014).
747
748 59 Sanchez-Martin, P. & Komatsu, M. p62/SQSTM1 - steering the cell through health and
749 disease. *J Cell Sci* **131**, jcs.222836 (2018).
750
751 60 Klionsky, D. J. *et al.* Guidelines for the use and interpretation of assays for monitoring
752 autophagy (3rd edition). *Autophagy* **12**, 1-222 (2016).
753
754 61 MacVicar, T. & Langer, T. OPA1 processing in cell death and disease - the long and
755 short of it. *J Cell Sci* **129**, 2297-2306 (2016).
756
757 62 Schiattarella, G. G. *et al.* Loss of Akap1 Exacerbates Pressure Overload-Induced Cardiac
758 Hypertrophy and Heart Failure. *Front Physiol* **9**, 558 (2018).
759
760 63 Schiattarella, G. G. *et al.* Akap1 Regulates Vascular Function and Endothelial Cells
761 Behavior. *Hypertension* **71**, 507-517 (2018).
762
763 64 Zhang, X., Tang, N., Hadden, T. J. & Rishi, A. K. Akt, FoxO and regulation of apoptosis.
764 *Biochim Biophys Acta* **1813**, 1978-1986, doi:10.1016/j.bbamcr.2011.03.010 (2011).
765 65 Brunet, A. *et al.* Akt promotes cell survival by phosphorylating and inhibiting a Forkhead
766 transcription factor. *Cell* **96**, 857-868 (1999).
767
768 66 Bouillet, P. *et al.* Proapoptotic Bcl-2 relative Bim required for certain apoptotic
769 responses, leukocyte homeostasis, and to preclude autoimmunity. *Science* **286**, 1735-
770 1738 (1999).
771
772 67 Willis, S. N. *et al.* Apoptosis initiated when BH3 ligands engage multiple Bcl-2
773 homologs, not Bax or Bak. *Science* **315**, 856-859 (2007).
774
775 68 Kirkland, R. A., Saavedra, G. M., Cummings, B. S. & Franklin, J. L. Bax regulates
776 production of superoxide in both apoptotic and nonapoptotic neurons: role of caspases. *J*
777 *Neurosci* **30**, 16114-16127 (2010).
778
779 69 Jiang, X., Jiang, H., Shen, Z. & Wang, X. Activation of mitochondrial protease OMA1 by
780 Bax and Bak promotes cytochrome c release during apoptosis. *Proc Natl Acad Sci U S A*
781 **111**, 14782-14787 (2014).
782
783 70 Karbowski, M. *et al.* Spatial and temporal association of Bax with mitochondrial fission
784 sites, Drp1, and Mfn2 during apoptosis. *J Cell Biol* **159**, 931-938 (2002).

785 71 Youle, R. J. & Strasser, A. The BCL-2 protein family: opposing activities that mediate
786 cell death. *Nat Rev Mol Cell Biol* **9**, 47-59 (2008).
787
788 72 Montessuit, S. *et al.* Membrane remodeling induced by the dynamin-related protein Drp1
789 stimulates Bax oligomerization. *Cell* **142**, 889-901 (2010).
790
791 73 Corredor, R. G. *et al.* Soluble adenylyl cyclase activity is necessary for retinal ganglion
792 cell survival and axon growth. *J Neurosci* **32**, 7734-7744 (2012).
793
794 74 Hellstrom, M. & Harvey, A. R. Cyclic AMP and the regeneration of retinal ganglion cell
795 axons. *Int J Biochem Cell Biol* **56**, 66-73 (2014).
796
797 75 Cueva Vargas, J. L., Belforte, N. & Di Polo, A. The glial cell modulator ibudilast
798 attenuates neuroinflammation and enhances retinal ganglion cell viability in glaucoma
799 through protein kinase A signaling. *Neurobiol Dis* **93**, 156-171 (2016).
800
801 76 Pryde, K. R., Smith, H. L., Chau, K. Y. & Schapira, A. H. PINK1 disables the anti-fission
802 machinery to segregate damaged mitochondria for mitophagy. *J Cell Biol* **213**, 163-171
803 (2016).
804
805 77 Joachim, S. C. *et al.* Retinal ganglion cell loss is accompanied by antibody depositions
806 and increased levels of microglia after immunization with retinal antigens. *PLoS One* **7**,
807 e40616 (2012).
808
809 78 Ju, W. K. *et al.* Increased mitochondrial fission and volume density by blocking
810 glutamate excitotoxicity protect glaucomatous optic nerve head astrocytes. *Glia* **63**, 736-
811 753 (2015).
812
813 79 Yoshida, M. *et al.* Overexpression of neurotrophin-3 stimulates a second wave of
814 dopaminergic amacrine cell genesis after birth in the mouse retina. *J Neurosci* **31**, 12663-
815 12673 (2011).
816
817 80 Perkins, G. *et al.* Electron tomography of neuronal mitochondria: three-dimensional
818 structure and organization of cristae and membrane contacts. *Journal of structural*
819 *biology* **119**, 260-272 (1997).
820
821
822
823
824
825
826
827

828 **Figure legend**

829 **Fig. 1 AKAP1 deficiency in glaucomatous RGCs.** (a) Western blot analysis for AKAP1 in the
830 retinas of 10-month-old glaucomatous DBA/2J and age-matched D2-*Gpnmb*$^+$ mice. (b)
831 Representative images from immunohistochemical analyses for AKAP1 (green) and TUJ1 (red)
832 in the retina of D2-*Gpnmb*$^+$ and glaucomatous DBA/2J mice. Arrowheads indicate accumulation
833 of AKAP1 co-labeled with TUJ1 in RGC somas and arrows indicate TUJ1-labeled axon bundles.
834 Note that glaucomatous RGCs showed decrease of AKAP1 protein expression. Blue color
835 indicates nucleus. (c) Quantitative analysis for fluorescent intensity showed a significant
836 decrease of AKAP1 immunoreactivity in the retina of glaucomatous DBA/2J mice. GCL,
837 ganglion cell layer; IPL, inner plexiform layer; INL, inner nuclear layer; OPL, outer plexiform
838 layer; ONL, outer nuclear layer. Mean ± SD; $n = 3$ (a) and $n = 10$ (c); $^*P < 0.05$ and $^{***}P <$
839 0.001 (two-tailed unpaired Student's *t*-test). Scale bar: 20 μm.

840

841 **Fig. 2 CaN-mediated dephosphorylation of Drp1 at S637 in glaucomatous retina.** (a)
842 Western blot analyses for CaN in the retinas of 10-month-old glaucomatous DBA/2J and age-
843 matched D2-*Gpnmb*$^+$ mice. (b) Representative images from immunohistochemical analyses for
844 CaN (green, arrowheads) co-labeled with RBPMS (red, arrowheads) in RGCs. Note that
845 glaucomatous RGCs showed increases of CaN protein expression. Blue color indicates nucleus.
846 (c) Quantitative analysis for fluorescent intensity showed a significant increase of CaN
847 immunoreactivity in the retina of glaucomatous DBA/2J mice. (d) Western blot analyses for
848 total Drp1 and phospho-Drp1 Ser637 in the retinas of glaucomatous DBA/2J and age-matched
849 D2-*Gpnmb*$^+$ mice. (e) Representative images from immunohistochemical analyses for total
850 Drp1 (green, arrowheads) co-labeled with TUJ1 (red, arrowheads) in RGCs. Note that
851 glaucomatous RGCs showed increases of total Drp1 protein expression. Blue color indicates
852 nucleus. (f) Quantitative analysis for fluorescent intensity showed a significant increase of Drp1
853 immunoreactivity in the retina of glaucomatous DBA/2J mice. GCL, ganglion cell layer; IPL,
854 inner plexiform layer; INL, inner nuclear layer; OPL, outer plexiform layer; ONL, outer nuclear
855 layer. Mean ± SD; $n = 3$ (a and d) and $n = 10$ (c and f); $^{**}P < 0.01$ and $^{***}P < 0.001$ (two-
856 tailed unpaired Student's *t*-test). Scale bar: 20 μm.

857

858 **Fig. 3 CaN expression in AKAP1$^{-/-}$ retina.** (a) Quantitative RT-PCR analysis for AKAP1 in
859 the retinas of AKAP1$^{-/-}$ and WT mice. (b) Western blot analysis for CaN in the retinas of
860 AKAP1$^{-/-}$ and WT mice. (c) Representative images from immunohistochemical analyses for
861 CaN (green, arrowheads) co-labeled with RBPMS (red, arrowheads) in RGCs. Note that
862 glaucomatous RGCs showed increases of CaN protein expression in the GCL and INL. Blue
863 color indicates nucleus. (d) Quantitative analysis for fluorescent intensity showed a significant
864 increase of CaN immunoreactivity in the retina of AKAP1$^{-/-}$ mice. GCL, ganglion cell layer;
865 IPL, inner plexiform layer; INL, inner nuclear layer; OPL, outer plexiform layer; ONL, outer
866 nuclear layer. Mean ± SD; $n = 3$ or 4 (a and b) and $n = 10$ (d); $^{**}P < 0.01$ and $^{***}P < 0.001$
867 (two-tailed unpaired Student's *t*-test). Scale bar: 20 μm.
868
869 **Fig. 4 Phosphorylation of AMPK at Thr172 and Drp1 at Ser637 in AKAP1$^{-/-}$ retina.** (a)
870 Western blot analysis for AMPK and phospho-AMPK Thr172 in the retinas of AKAP1$^{-/-}$ and
871 WT mice. (b) Western blot analysis for total Drp1, phospho-Drp1 Ser637 and phospho-Drp1
872 Ser616 in the retinas of AKAP1$^{-/-}$ and WT mice. (c) Representative images from
873 immunohistochemical analyses for total Drp1 (green, arrowheads) co-labeled with RBPMS (red,
874 arrowheads) in RGCs. Note that glaucomatous RGCs showed an increase of total Drp1 protein
875 expression in RGCs. Blue color indicates nucleus. (d) Quantitative analysis for fluorescent
876 intensity showed a significant increase of Drp1 immunoreactivity in the retina of AKAP1$^{-/-}$ mice.
877 GCL, ganglion cell layer; IPL, inner plexiform layer; INL, inner nuclear layer; OPL, outer
878 plexiform layer; ONL, outer nuclear layer. Mean ± SD; $n = 3$ or 6 (a) and $n = 10$ (d); $^{*}P < 0.05$
879 (two-tailed unpaired Student's *t*-test). Scale bar: 20 μm.
880
881 **Fig. 5 Mitochondrial fission in AKAP1$^{-/-}$ RGC somas.** (a) Quantitative RT-PCR analyses for
882 OPA1 and Mfn1 and Western blot analysis for total OPA1 (L-OPA1 & S-OPA1), and Mfn1 and
883 2 in the retinas of AKAP1$^{-/-}$ and WT mice. (b-d) EM and EM tomography analyses for
884 mitochondrial fission and loss in AKAP1$^{-/-}$ RGC somas. (b) 1.6-nm thick slices through the
885 middle of tomographic volumes of WT RGC somas show an abundance of larger mitochondria.
886 In contrast, the mitochondria are smaller with a greater number in AKAP1$^{-/-}$ RGC somas, but
887 show no alteration of cristae architecture. (c) Quantitative analyses of mitochondrial volume
888 density, number and cross-sectional area and cristae abundance in WT and AKAP1$^{-/-}$ RGC

889 somas. Note that AKAP1$^{-/-}$ RGC somas show significant loss of mitochondrial mass and cross-
890 sectional area, and a significant increase in mitochondrial number. However, there was no
891 significant difference in cristae abundance of AKAP1$^{-/-}$ RGC somas. (d) Top view of the
892 surface-rendered volume showing 3 adjacent mitochondria from a WT tomographic volume
893 (left) and an AKAP1$^{-/-}$ volume (right). Comparing the side view with the top view provides
894 perspective on the distribution of the predominantly tubular cristae (in an assortment of colors)
895 and reveals substantial heterogeneity of cristae size. The mitochondrial outer membranes were
896 made translucent to better visualize the cristae. The number of cristae in each mitochondrion is
897 indicated. Mean ± SD (a) and Mean ± SEM (c); $n = 3$ (a), $n = 11$ (mitochondrial volume,
898 number and cristae abundance for WT and AKAP1$^{-/-}$, c) and $n = 22$ or 39 (mitochondrial size for
899 WT or AKAP1$^{-/-}$, c); $*P < 0.05$ and $**P < 0.01$ (two-tailed unpaired Student's *t*-test). Scale
900 bars: 200 nm.
901
902 **Fig. 6 Mitophagosome formation in AKAP1$^{-/-}$ RGC somas.** (a) Western blot analyses for
903 LC3 and p62 in the retinas of AKAP1$^{-/-}$ and WT mice. (b) Representative images from
904 immunohistochemical analyses for LC3 (green) co-labeled with TUJ1 (red) in RGCs and their
905 axons. Note that LC3 immunoreactivity was localized in RGC somas (arrowheads) and their
906 axons (arrows) in WT and AKAP1$^{-/-}$ retina. Blue color indicates nucleus. GCL, ganglion cell
907 layer; IPL, inner plexiform layer; INL, inner nuclear layer; OPL, outer plexiform layer; ONL,
908 outer nuclear layer. Scale bar, 20 μm. (c-j) EM tomography and 3D reconstruction analysis.
909 (c) A 1.6 nm-thick slice through the tomographic volume of the RGC showing an
910 autophagosome with a degenerating mitochondrial fragment inside. A mitochondrion is nearby
911 with a strand of ER positioned in between the autophagosome and mitochondrion. ER is
912 typically involved with mitochondrial fission. The double membrane of the autophagosome is
913 only partially visualized and so is indicated by white arrowheads on opposite sides. For
914 comparison, the double membrane of the mitochondrial periphery is indicated by black
915 arrowheads on opposite sides to emphasize that the spacing between individual autophagosomal
916 membranes is about the same as the spacing between individual mitochondrial peripheral
917 membranes, as it should be. Labels: A, autophagosome; M, mitochondrion; PM, RGC plasma
918 membrane; ER, endoplasmic reticulum strand. Scale = 200 nm. (d) Another slice through the
919 RGC volume showing a small stretch of clearly separated components of the autophagosomal

920 double membrane (white arrowheads). For comparison, the spacing of the mitochondrial double
921 membrane is indicated by the black arrowheads. (e) A third slice through the RGC volume that
922 best shows the double membrane of the mitochondrial fragment (white arrowheads) inside the
923 autophagosome. Perhaps the reason that less than half the mitochondrial double membrane is
924 seen is because it was being degraded at the time the tissue was fixed. The spacing between the
925 individual membranes of the fragment is the same as the spacing between the individual
926 membranes of the mitochondrion (black arrowheads). (f) Side view with the mitophagosome
927 membrane made transparent to see the engulfed mitochondrion. (g) Side view with the outer
928 mitochondrial membrane made transparent to see the 2 fragments of the inner boundary
929 membrane (IBM) and the one crista that remain. (h) Top view showing the crista and right-hand
930 portion of the IBM inside the mitochondrion, which is inside the mitophagosome. (i and j) An
931 oblique view with the mitophagosome and outer mitochondrial membranes made transparent to
932 see the crista and two IBM fragments. Note that mitochondria in the AKAP1$^{-/-}$ RGC soma
933 demonstrate autophagosome/mitophagosome formation. Mean ± SD; $n = 3$ or 4 (a); $*P < 0.05$
934 and $**P < 0.01$ (two-tailed unpaired Student's *t*-test). Scale bar: 500 nm
935
936 **Fig. 7 OXPHOS dysfunction and oxidative stress in AKAP1$^{-/-}$ retinas.** (a) Western blot
937 analyses for OXPHOS Cxs in the retinas of AKAP1$^{-/-}$ and WT mice. (b) Western blot analyses
938 for SOD2 in the retinas of AKAP1$^{-/-}$ and WT mice. (c) Representative images from
939 immunohistochemical analyses for SOD2 (green, arrowheads) co-labeled with Brn3a (red,
940 arrowheads) in the retina. Note that AKAP1$^{-/-}$ retina shows increases of SOD2 protein
941 expression in the inner retinal layer compared with WT retina. Blue color indicates nucleus. (d)
942 Quantitative analysis for fluorescent intensity showed a significant increase of SOD2
943 immunoreactivity in the retina of AKAP1$^{-/-}$ mice. GCL, ganglion cell layer; IPL, inner plexiform
944 layer; INL, inner nuclear layer; OPL, outer plexiform layer; ONL, outer nuclear layer.
945 Mean ± SD; $n = 4$ or 10 (a), $n = 4$ (b) and $n = 10$ (d). $*P < 0.05$, $**P < 0.01$ and $***P < 0.001$
946 (two-tailed unpaired Student's *t*-test). Scale bar: 20 μm.
947
948 **Fig. 8 Akt inactivation and Bim/Bax activation in AKAP1$^{-/-}$ retinas.** (a) Western blot
949 analyses for Akt, phospho-Akt Ser473 and phospho-Akt Thr308 in the retinas of AKAP1$^{-/-}$ and
950 WT mice. (b) Representative images from immunohistochemical analyses for Akt (green,

951 arrowheads) co-labeled with Brn3a (red, arrowheads) in the retina. Note that AKAP1$^{-/-}$ retina
952 show increases of Akt protein expression in the INL and GCL compared with WT retina. Blue
953 color indicates nucleus. (c) Quantitative analysis for fluorescent intensity showed a significant
954 increase of Akt immunoreactivity in the retina of AKAP1$^{-/-}$ mice. (d) Western blot analyses for
955 Bim and Bax in the retinas of AKAP1$^{-/-}$ and WT mice. (e) Representative images from
956 immunohistochemical analyses for Bax (green, arrowheads) co-labeled with RBPMS (red,
957 arrowheads) in the retina. Note that AKAP1$^{-/-}$ retina show increases of Bax protein expression in
958 the GCL compared with WT retina. Blue color indicates nucleus. (f) Quantitative analysis for
959 fluorescent intensity showed a significant increase of Bax immunoreactivity in the retina of
960 AKAP1$^{-/-}$ mice. GCL, ganglion cell layer; IPL, inner plexiform layer; INL, inner nuclear layer;
961 OPL, outer plexiform layer; ONL, outer nuclear layer. Mean ± SD; n = 3 or 4 (a and d) and n =
962 10 (c and f). *$P < 0.05$, **$P < 0.01$ and ***$P < 0.001$ (two-tailed unpaired Student's t-test).
963 Scale bar: 20 μm.

Figure 1.

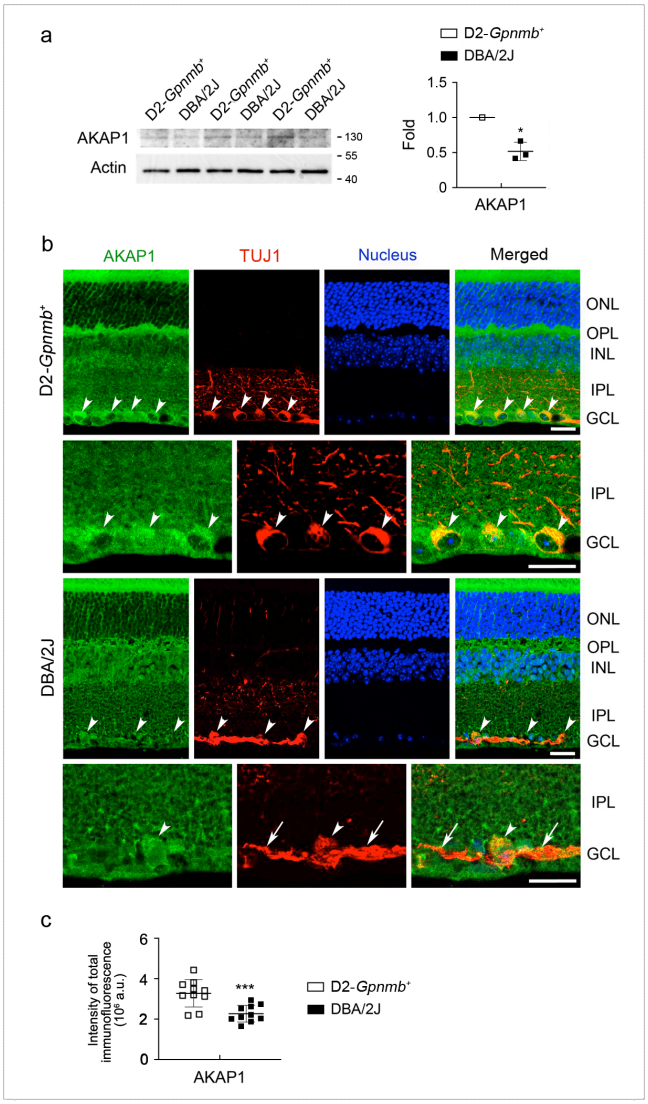
a
D2-Gpnmb+
DBA/2J
D2-Gpnmb+
DBA/2J
D2-Gpnmb+
DBA/2J
D2-Gpnmb+
DBA/2J
AKAP1
Actin
130
55
40
Fold
1.5
1.0
0.5
0
*
AKAP1
b
AKAP1
TUJ1
Nucleus
Merged
D2-Gpnmb+
DBA/2J
ONL
OPL
INL
IPL
GCL
IPL
GCL
ONL
OPL
INL
IPL
GCL
IPL
GCL
c
Intensity of total immunofluorescence (10⁶ a.u.)
6
4
2
0
***
AKAP1
D2-Gpnmb+
DBA/2J

Figure 2.

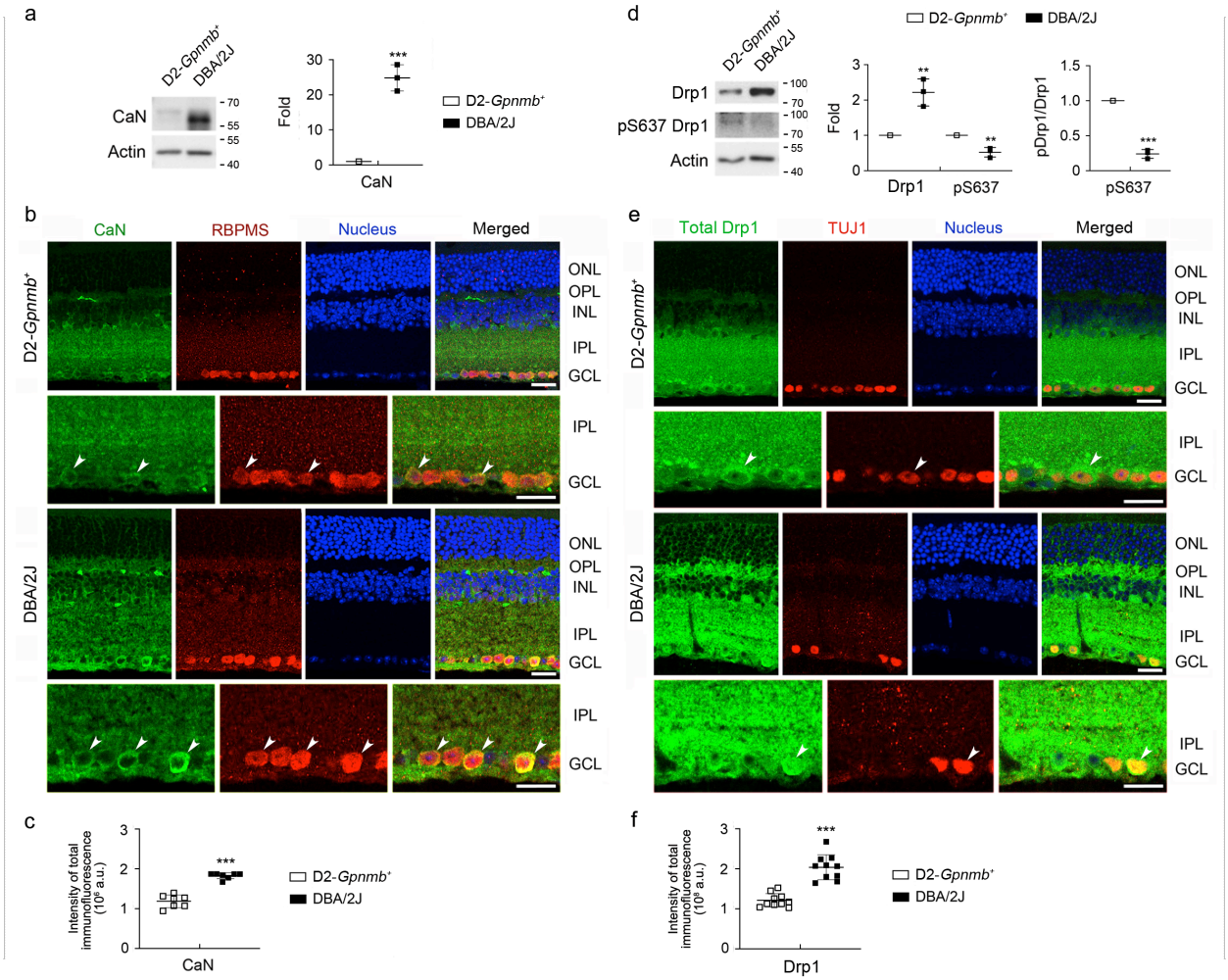
a
D2-Gpnmb+
DBA/2J
CaN
Actin
70
55
55
40
Fold
30
20
10
0
***
CaN
D2-Gpnmb+
DBA/2J
d
D2-Gpnmb+
DBA/2J
Drp1
pS637 Drp1
Actin
100
70
100
70
55
40
Fold
3
2
1
0
**
**
Drp1
pS637
pDrp1/Drp1
1.5
1.0
0.5
0
***
pS637
b
CaN
RBPMS
Nucleus
Merged
D2-Gpnmb+
DBA/2J
ONL
OPL
INL
IPL
GCL
e
Total Drp1
TUJ1
Nucleus
Merged
D2-Gpnmb+
DBA/2J
ONL
OPL
INL
IPL
GCL
c
Intensity of total immunofluorescence (10⁸ a.u.)
3
2
1
0
***
CaN
D2-Gpnmb+
DBA/2J
f
Intensity of total immunofluorescence (10⁸ a.u.)
3
2
1
0
***
Drp1
D2-Gpnmb+
DBA/2J

Figure 3.

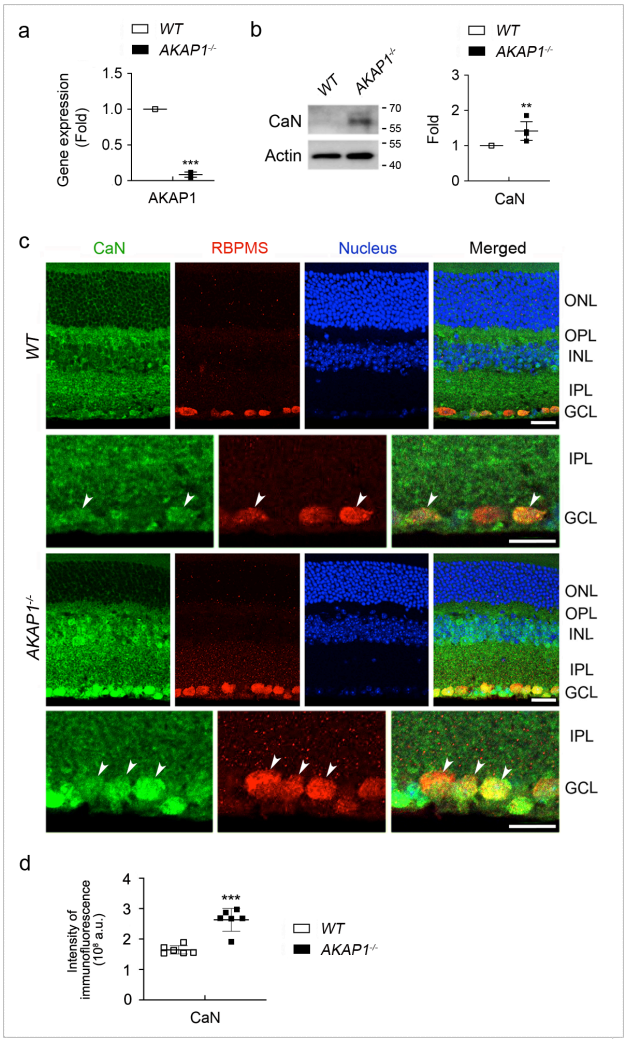
a
WT
AKAP1-/-
Gene expression (Fold)
1.5
1.0
0.5
0
***
AKAP1
b
WT
AKAP1-/-
CaN
Actin
70
55
55
40
WT
AKAP1-/-
Fold
3
2
1
0
**
CaN
c
CaN
RBPMS
Nucleus
Merged
WT
ONL
OPL
INL
IPL
GCL
IPL
GCL
AKAP1-/-
ONL
OPL
INL
IPL
GCL
IPL
GCL
d
Intensity of immunofluorescence (10⁸ a.u.)
4
3
2
1
0
***
CaN
WT
AKAP1-/-

Figure 4.

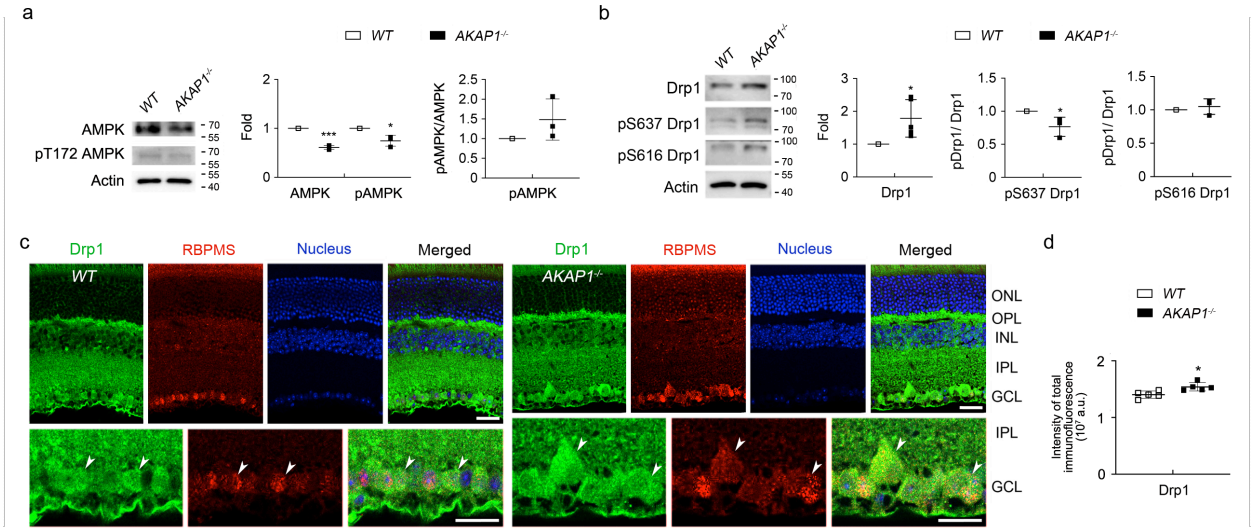
a
WT
AKAP1-/-
AMPK
pT172 AMPK
Actin
Fold
AMPK
pAMPK
pAMPK/AMPK
b
Drp1
pS637 Drp1
pS616 Drp1
pDrp1/ Drp1
c
Drp1
RBPMS
Nucleus
Merged
ONL
OPL
INL
IPL
GCL
d
Intensity of total immunofluorescence (10⁷ a.u.)

Figure 5.

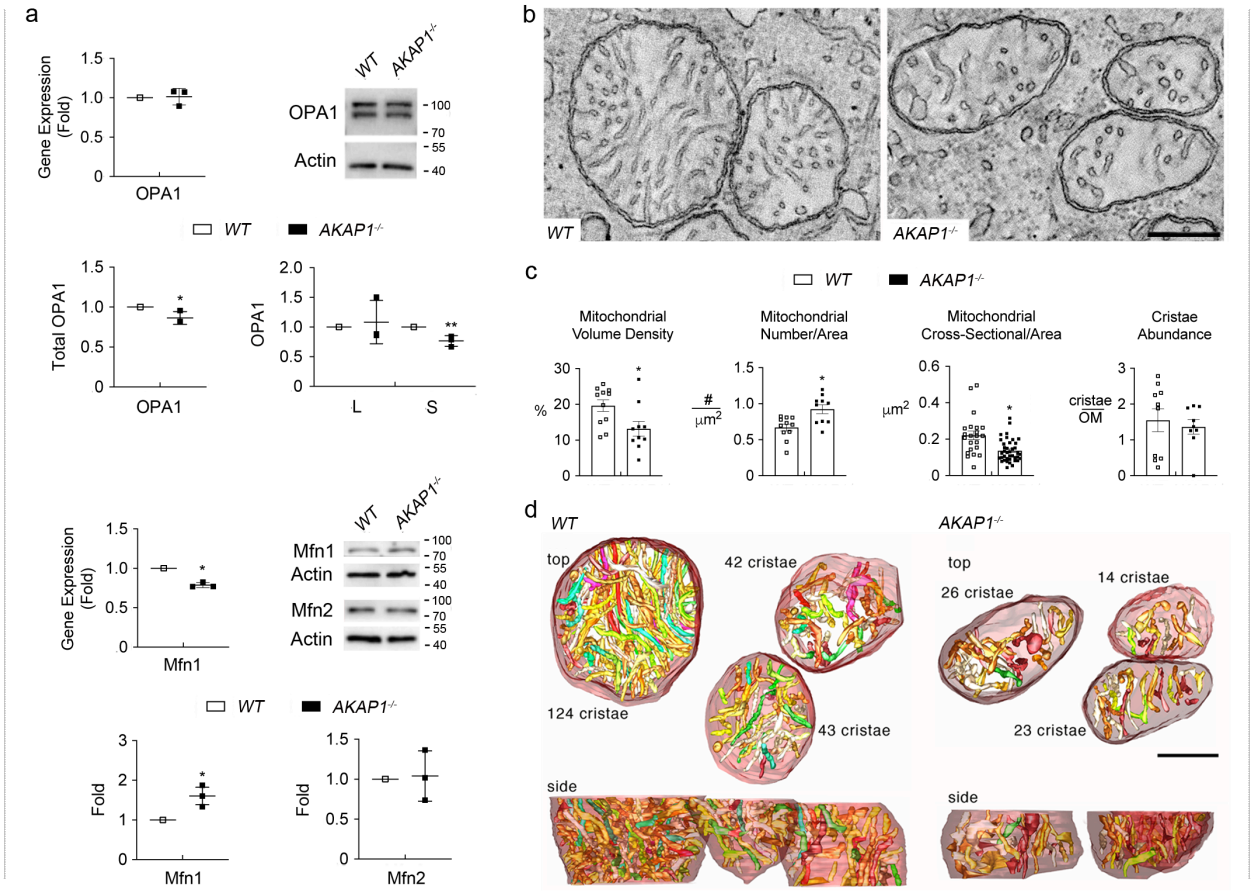
a
Gene Expression (Fold)
OPA1
WT
AKAP1-/-
Actin
Total OPA1
L
S
Mfn1
Mfn2
Fold
b
WT
AKAP1-/-
c
Mitochondrial Volume Density
Mitochondrial Number/Area
Mitochondrial Cross-Sectional/Area
Cristae Abundance
d
top
side
42 cristae
124 cristae
43 cristae
26 cristae
14 cristae
23 cristae

Figure 6.

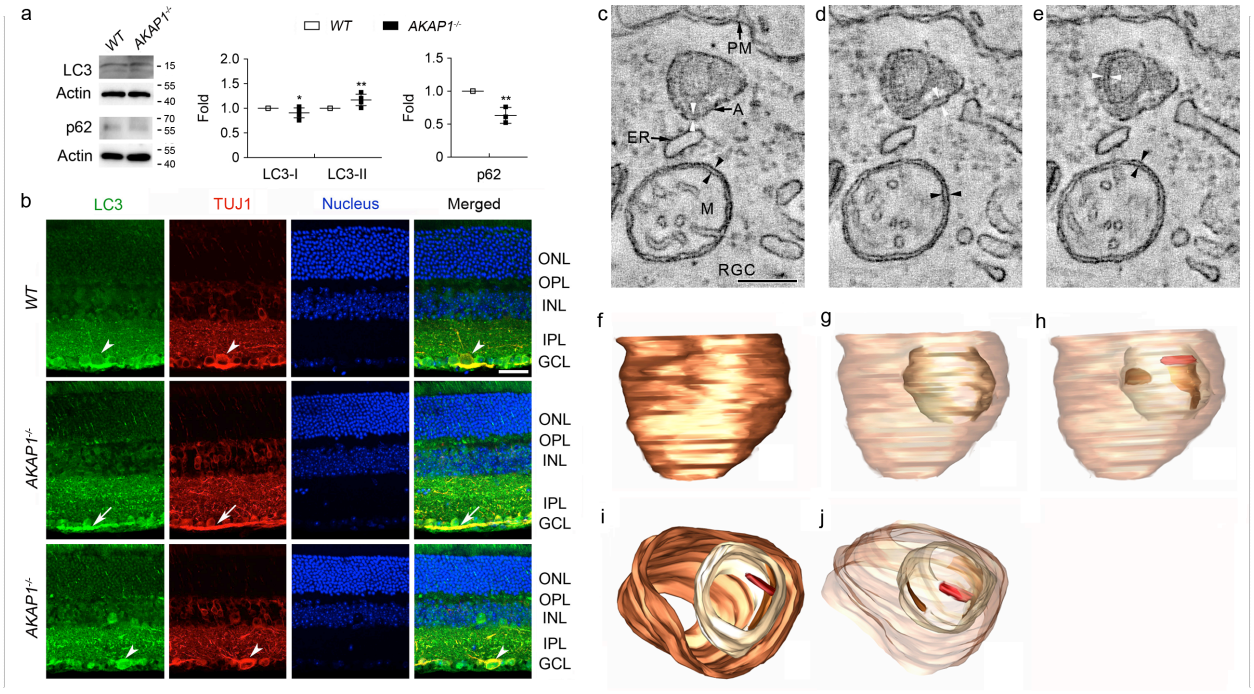
a
WT
AKAP1-/-
LC3
Actin
p62
Actin
15
55
40
70
55
55
40
WT
AKAP1-/-
Fold
2.0
1.5
1.0
0.5
0
LC3-I
LC3-II
p62
b
LC3
TUJ1
Nucleus
Merged
WT
AKAP1-/-
AKAP1-/-
ONL
OPL
INL
IPL
GCL
c
d
e
PM
A
ER
M
RGC
f
g
h
i
j

Figure 7.

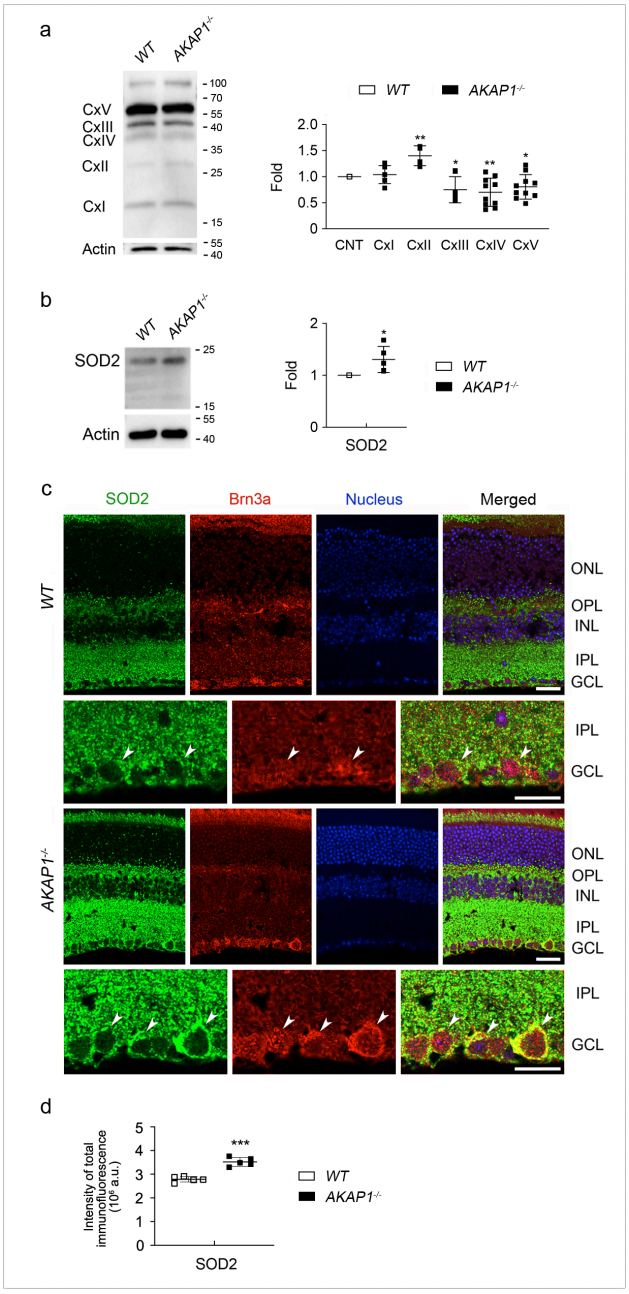
a
WT
AKAP1-/-
CxV
CxIII
CxIV
CxII
CxI
Actin
100
70
55
40
35
25
15
55
40
WT
AKAP1-/-
Fold
2.0
1.5
1.0
0.5
0
CNT
CxI
CxII
CxIII
CxIV
CxV
b
WT
AKAP1-/-
SOD2
Actin
25
15
55
40
Fold
2
1
0
SOD2
WT
AKAP1-/-
c
SOD2
Brn3a
Nucleus
Merged
WT
AKAP1-/-
ONL
OPL
INL
IPL
GCL
d
Intensity of total immunofluorescence (10⁶ a.u.)
5
4
3
2
1
0
SOD2
WT
AKAP1-/-

Figure 8.

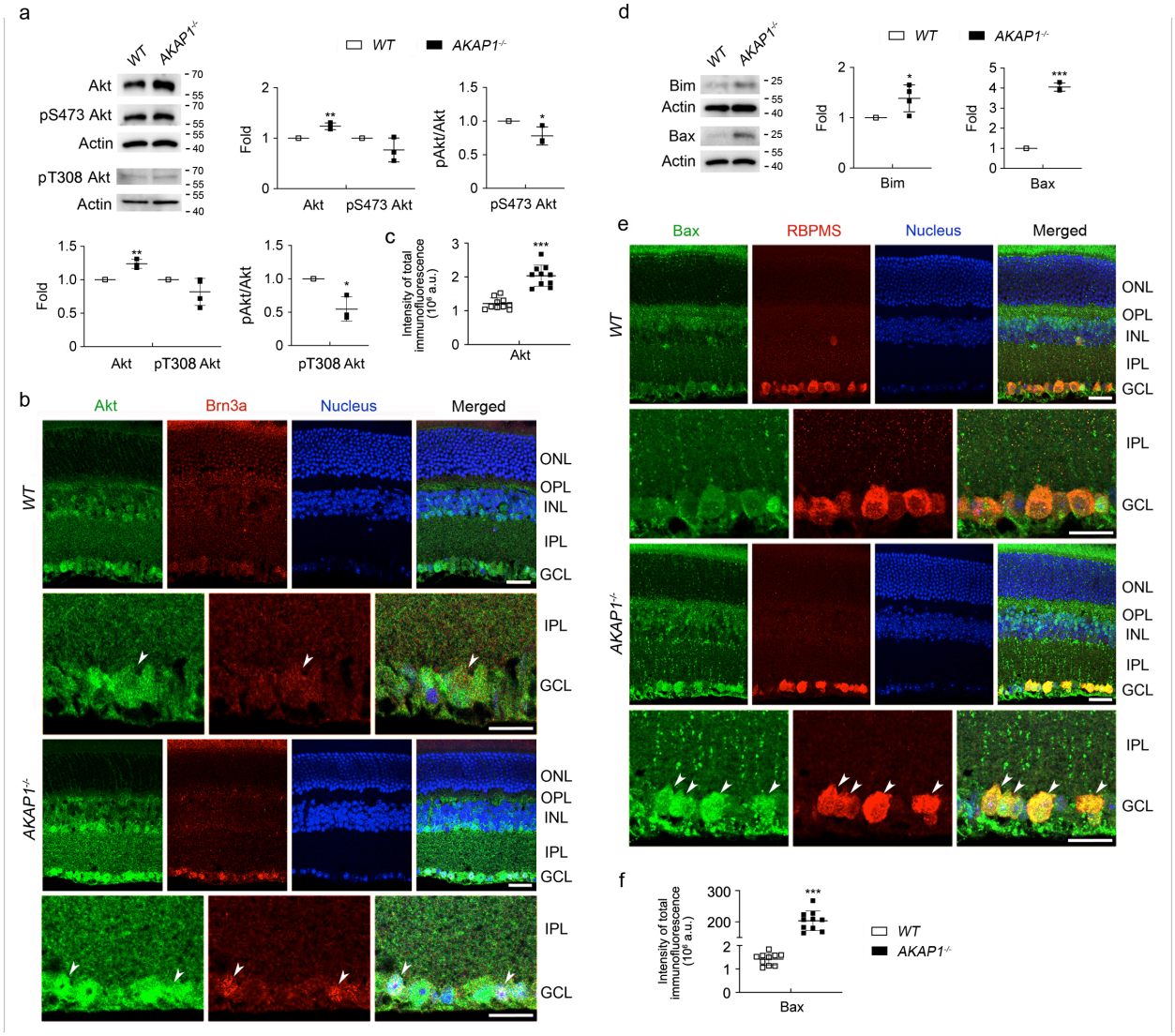
a
WT
AKAP1-/-
Akt
pS473 Akt
Actin
pT308 Akt
Actin
Fold
pAkt/Akt
Akt
pS473 Akt
pT308 Akt
c
Intensity of total immunofluorescence (10⁶ a.u.)
b
Akt
Brn3a
Nucleus
Merged
ONL
OPL
INL
IPL
GCL
d
Bim
Bax
e
RBPMS
f